

# BESIII Analysis Memo

BAM-00XXX

June 29, 2016

1     **The Measurements of  $R$  value in  $e^+e^-$  Annihilation at Center-of-Mass**  
2     **Energy from 2.2324 to 3.671 GeV at BESIII**

3     Z. Gao<sup>a</sup>, B. X. Zhang<sup>b</sup>, C. Geng<sup>a</sup>, W. P. Wang<sup>a</sup>, Y. T. Li<sup>b</sup>, L. Xia<sup>a</sup>, X. A. Xiong<sup>b</sup>, X. Y. Zhou<sup>b</sup>,  
4     Y. Q. Wang<sup>c</sup>, Y. P. Guo<sup>c</sup>, C. F. Redmer<sup>c</sup>, Z. Q. Liu<sup>c</sup>, A. Denig<sup>c</sup>, W. B. Yan<sup>a</sup>, R. G. Ping<sup>b</sup>,  
5     Z. Y. Wang<sup>b</sup>, H. M. Hu<sup>b</sup>, G. S. Huang<sup>a</sup>, Z. G. Zhao<sup>a</sup>

6                     <sup>a</sup>*University of Science and Technology of China*

7                     <sup>b</sup>*Institute of High Energy Physics*

8                     <sup>c</sup>*Johannes Gutenberg University of Mainz*

9                     **Abstract**

10                    Using data samples collected with BESIII detector operating at BEPCII storage ring, the  
11                     $R = \sigma(e^+e^- \rightarrow \text{hadrons})/\sigma(e^+e^- \rightarrow \mu^+\mu^-)$  is measured at 14 energy points in the continuum  
12                    region from the center-of-mass energies  $\sqrt{s} = 2.2324$  to 3.671 GeV. The average uncertainty  
13                    of  $R$  values is about 3%, which is dominated by the systematic uncertainty.

1	<b>Contents</b>	
2	<b>1 Introduction</b>	<b>2</b>
3	<b>2 The BESIII Detector</b>	<b>2</b>
4	<b>3 Data Sets and Monte Carlo Simulation</b>	<b>2</b>
5	3.1 Data Sets . . . . .	2
6	3.2 Monte Carlo Simulation . . . . .	3
7	<b>4 Event Selection</b>	<b>4</b>
8	4.1 Rejection of Bhabha and Di-gamma Events . . . . .	5
9	4.2 Good Track Selection . . . . .	5
10	4.3 Good Hadronic Event . . . . .	9
11	<b>5 Determination of number of hadronic events</b>	<b>11</b>
12	5.1 Beam-associated Backgrounds . . . . .	11
13	5.2 QED Backgrounds . . . . .	11
14	5.3 Treatment of data samples at 3.65 GeV . . . . .	14
15	<b>6 Comparisons Between Data and Monte Carlo</b>	<b>14</b>
16	<b>7 Detection Efficiency</b>	<b>16</b>
17	<b>8 The Initial State Radiation Correction</b>	<b>21</b>
18	8.1 The ISR Correction . . . . .	21
19	8.2 The Numerical Results . . . . .	22
20	<b>9 Systematic Uncertainty</b>	<b>25</b>
21	9.1 Event Selection . . . . .	25
22	9.2 Luminosity . . . . .	26
23	9.3 Generator Model . . . . .	26
24	9.4 Radiation Correction . . . . .	26
25	9.5 Trigger Efficiency . . . . .	26
26	9.6 Total Systematic Uncertainty . . . . .	26
27	<b>10 Results</b>	<b>28</b>
28	<b>11 Summary</b>	<b>30</b>

## 1 Introduction

In precision tests of the Standard Model (SM), the quantities  $\alpha(M_Z^2)$ , the QED running coupling constant evaluated at the Z pole, and  $a_\mu = (g - 2)/2$ , the anomalous magnetic moment of the muon, are of fundamental importance. The dominant uncertainties in both  $\alpha(M_Z^2)$  and  $a_\mu$  are due to the effects of hadronic vacuum polarization, which cannot be reliably calculated in the low energy region (below 5 GeV) [1]-[4]. In these studies, hadronic cross sections ( $R$  value) are used as the input parameters in the calculations of the radiation corrections (vacuum polarization and vertex correction), where  $R$  is the lowest order cross section for  $e^+e^- \rightarrow$  hadrons in units of the lowest order QED cross section for  $e^+e^- \rightarrow \mu^+\mu^-$ . Namely,  $R = \sigma(e^+e^- \rightarrow \text{hadrons})/\sigma(e^+e^- \rightarrow \mu^+\mu^-)$ , where  $\sigma(e^+e^- \rightarrow \mu^+\mu^-) = 4\pi\alpha^2(0)/3s = 86.8 \text{ nb}/s(\text{GeV}/c)$ .

In experiment,  $R$  value is determined by

$$R = \frac{N_{had}^{obs} - N_{bkg}}{\sigma_{\mu\mu}^0 \cdot \mathcal{L} \cdot \varepsilon_{had} \cdot \varepsilon_{trig} \cdot (1 + \delta)}, \quad (1)$$

where  $N_{had}^{obs}$  is the number of observed hadronic events,  $N_{bkg}$  is the number of background events,  $\mathcal{L}$  is the integrated luminosity,  $\varepsilon_{had}$  is the detection efficiency for hadron event selection,  $\varepsilon_{trig}$  is the trigger efficiency,  $1 + \delta$  is the initial state radiation (ISR) correction factor, and  $\sigma_{\mu\mu}^0$  is the Born-level cross section for  $e^+e^- \rightarrow \mu^+\mu^-$ .

Several experiments contributed to the  $R$  measurement in the energy range between 2 and 5 GeV [1]-[8]. The precision of these measurements is generally around 6.6% for all experiments except BESII [7] and KEDR [8] at a few energy points, where the accuracy of about 3.3% was reached. It should be noted that systematic uncertainties dominate the  $R$  measurements for these two experiments.

In this analysis, the values of  $R$  between 2.2324 and 3.671 GeV are presented, with an average precision less than 3% at most of the energy points.

## 2 The BESIII Detector

BEPCII [9] is a double-ring  $e^+e^-$  collider designed to provide a peak luminosity of  $10^{33} \text{ cm}^{-2}\text{s}^{-1}$  at the center-of-mass ( $\sqrt{s}$ ) energy of 3770 MeV. The BESIII [10] detector has a geometrical acceptance of 93% of  $4\pi$  and has four main components: (1) A small-cell, helium-based (60% He, 40% C<sub>3</sub>H<sub>8</sub>) main drift chamber (MDC) with 43 layers providing an average single-hit resolution of 135  $\mu\text{m}$ , and charged-particle momentum resolution in a 0.9 or 1.0 T magnetic field of 0.5% at 1 GeV/ $c$ . (2) An electromagnetic calorimeter (EMC) consisting of 6240 CsI(Tl) crystals in cylindrical structure has one barrel and two end-caps. The energy resolution at 1.0 GeV/ $c$  is 2.5% (5%) in the barrel (endcaps), and the position resolution is 6 mm (9 mm) in the barrel (endcaps). (3) Particle Identification is provided by a time-of-flight system (TOF) constructed of 5-cm-thick plastic scintillators, with 176 detectors of 2.4 m length in two layers in the barrel and 96 fan-shaped detectors in the endcaps. The barrel (endcap) time resolution of 80 ps (110 ps) provides  $2\sigma K/\pi$  separation for momenta up to  $\sim 1.0 \text{ GeV}/c$ . (4) A muon system (MUC) consists of 1000 m<sup>2</sup> of resistive plate chambers in nine (eight) layers of barrel (endcap) which provides 2 cm position resolution.

## 3 Data Sets and Monte Carlo Simulation

### 3.1 Data Sets

This analysis is based on the data samples collected with the BESIII [10] detector operating at BEPCII [9]. Table 1 summarizes useful information for the data sets.

Table 1: Data samples used for  $R$  measurement at BESIII

	$E_{cm}(\text{GeV})$	Run range	Integrated luminosity ( $\text{pb}^{-1}$ )	Purpose
1	2.2324	28624 – 28648	2.645	R scan
2	2.4000	28577 – 28621	3.415	R scan
3	2.8000	28553 – 28575	3.753	R scan
4	3.0500	28312 – 28346	14.893	$J/\psi$ scan
5	3.0600	28347 – 28381	15.040	$J/\psi$ scan
6	3.0800	27147 – 27233, 28241 – 28266	31.019	$J/\psi$ scan
7	3.4000	28543 – 28548	1.733	R scan
8	3.5000	33725 – 33733	3.633	off $\psi(3770)$
9	3.5424	24983 – 25015, 33734 – 33743	8.693	$\tau$ mass scan
10	3.5538	25016 – 25094	5.562	$\tau$ mass scan
11	3.5611	25100 – 25141	3.847	$\tau$ mass scan
12	3.6002	25143 – 25243	9.502	$\tau$ mass scan
13	3.6500	33747 – 33758	4.760	off $\psi(3686)$
14	3.6710	33759 – 33764	4.628	off $\psi(3770)$

### 3.2 Monte Carlo Simulation

The optimization of event selection and the estimation of the background events are performed through Monte Carlo (MC) simulations. The GEANT4-based simulation software BOOST [16] includes the geometric description of the BESIII detectors and the current analysis is performed with BOSS6.6.4.p01.

In order to determine detection efficiency, two generators are used, respectively. One is ConExc [17] for  $e^+e^- \rightarrow \text{hadrons}$ . This generator is constructed within the framework of BesEvtGen. It provides momentum for each final state to do the detection simulation, and provide the ISR factor and vacuum polarization factors for user to undress the observed cross section. Another is LUARLW, which uses a formalism based on the Lund Area Law model, but without the extreme-high-energy approximations used in JETSET's string fragmentation algorithm [7, 20].

The simulated hadronic events are weighted with number of good tracks and clusters, which is described in appendix ??.

For the estimation of background events, the generators Babayaga v3.5 [11] for Bhabha, Di-gamma and  $e^+e^- \rightarrow \mu^+\mu^-$ , generator KKMC [12] for  $e^+e^- \rightarrow \tau^+\tau^-$  and BesTwoGam [13] for  $e^+e^- \rightarrow e^+e^- + X$  ( $X$  can be hadrons or leptons) are used, respectively. The size of MC samples for each process at 2.2324 GeV is listed in Table 2, and information on the generator model and the size of MC at other energy points is listed in appendix ??.

Table 2: MC samples used for  $R$  measurement at 2.2324 GeV

Sort	Process	Generator	$N_{event}$ (million)
1	$e^+e^- \rightarrow \text{hadrons}$	ConExc	0.5
2	Bhabha	babayaga v3.5	5.0
3	Di-gamma	babayaga v3.5	1.0
4	$e^+e^- \rightarrow \mu^+\mu^-$	babayaga v3.5	1.0
5	$e^+e^- \rightarrow e^+e^- + X$	BesTwogam	1.0
6	$e^+e^- \rightarrow \tau^+\tau^-$	KKMC	-

## 4 Event Selection

The events are selected in three steps. The first is the rejection of Bhabha and Di-gamma events using the EMC information only, since their cross sections are large and they are main QED background events. The second is the determination of good hadronic tracks in an event. The third step is to reconstruct the hadronic event with further requirements. The detailed selection criteria are given in the subsequent sections.

Figure 1 is the flow diagram for hadronic event selection.

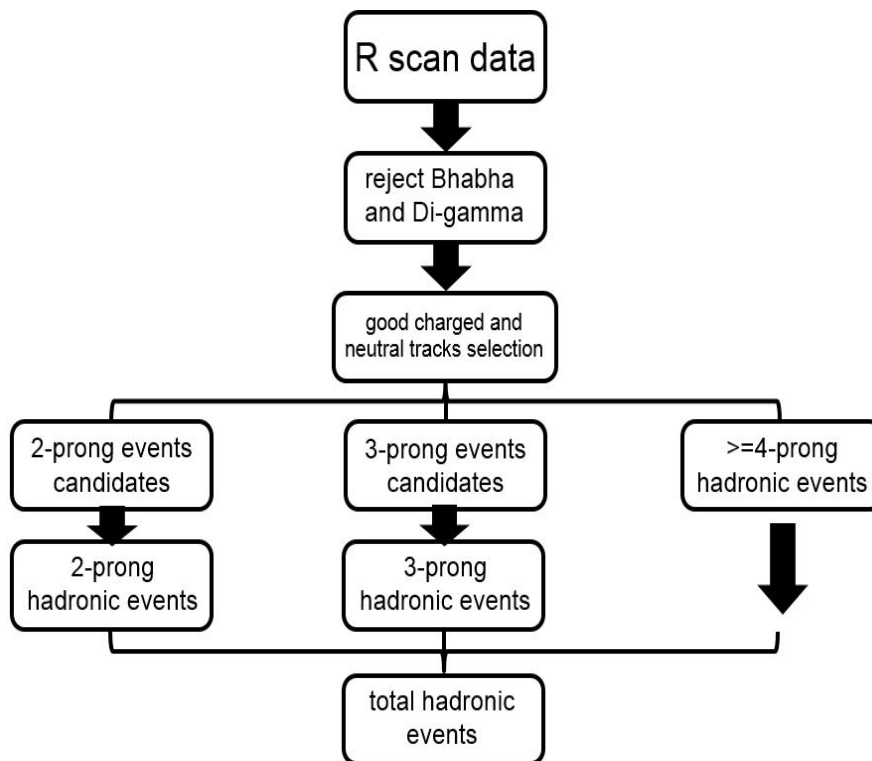


Figure 1: The diagram of hadronic event selection.

## 4.1 Rejection of Bhabha and Di-gamma Events

Bhabha and Di-gamma events are characterized by large energy depositions in EMC and the back-to-back tracks. Bhabha events are not exactly back-to-back in the azimuthal angle due to the curvature in the magnetic field. However, both of them are back-to-back in the polar angle.

An event is determined to be a Bhabha or Di-gamma event if it satisfies the following selection procedure:

- There are at least two showers in the event and the largest two deposited energies of these showers are picked out.
- The energy deposition of secondary energetic shower is required to be larger than  $0.65 \times E_{beam}$ , where  $E_{beam}$  represents the beam energy.
- The absolute  $\Delta\theta$  is required to be less than 10 degrees, where  $|\Delta\theta| = |\theta_1 + \theta_2 - 180^\circ|$ ,  $\theta$  is the polar angle in EMC.

Figure 2 shows the distributions of  $|\Delta\theta|$  with two energy depositions larger than  $0.65 \times E_{beam}$  at 2.4 GeV.

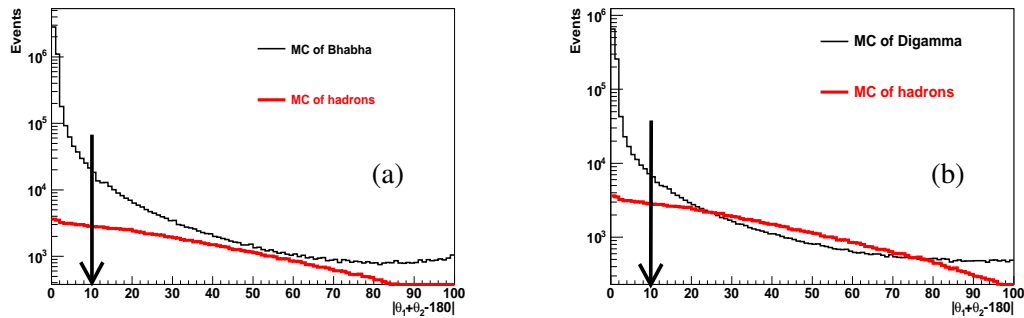


Figure 2: Distributions of  $|\Delta\theta|$ . Black histograms are MC of Bhabha (left) and MC of Digamma (right), red histograms are MC of hadrons.

Figure 3 shows the scatter plot of  $|\Delta\theta|$  versus energy deposition at 2.4 GeV. Events in blue boxes are regarded as Bhabha or Di-gamma events which are vetoed.

## 4.2 Good Track Selection

If an event is determined not to be Bhabha or Di-gamma, the number of good hadronic tracks in the event is counted.

- Each charged track must locate within  $V_r = \sqrt{V_x^2 + V_y^2} < 1.0$  cm, where  $V_x, V_y$  are the x, y coordinates of the point of closest approach to the run-dependent interaction point respectively.
- The track should lie within the polar angle region  $|\cos\theta| < 0.93$  within the detector acceptance.
- Momentum of each track is required to be smaller than  $0.94 \times p_{beam}$  which removes the tracks with the momenta close to the beam energy (tracks from some 2-body processes or beam, since

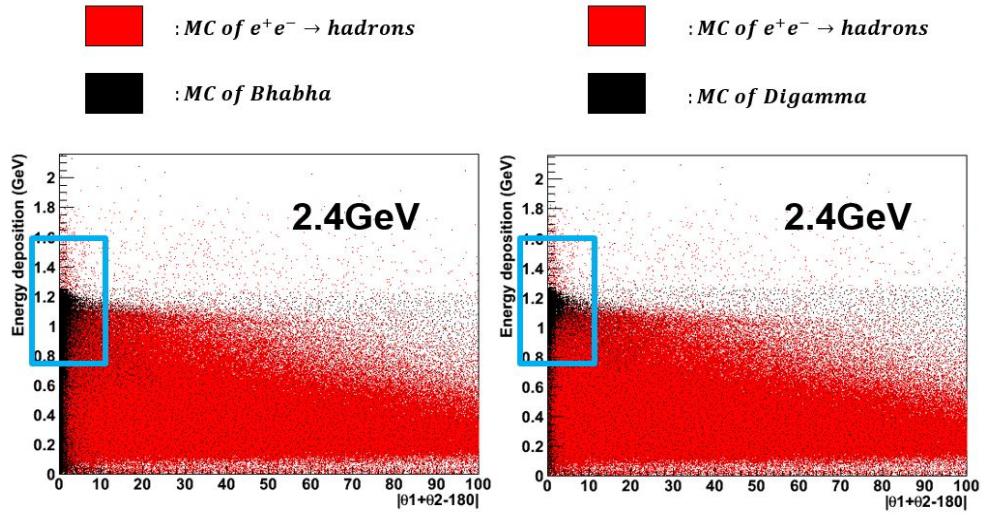


Figure 3: Scatter plot of  $|\Delta\theta|$  versus energy deposition. Black dots are signal MC and red ones are MC of Bhabha (left) and Di-gamma (right).

1 they are to be removed anyway). Here  $p_{beam}$  represents the momentum of beam and the factor 0.94  
 2 is 3 times standard deviation from maximum momentum.  
 3 Figure 4 shows the distribution of momentum for tracks without maximum momentum require-  
 4 ment at 2.4 GeV.

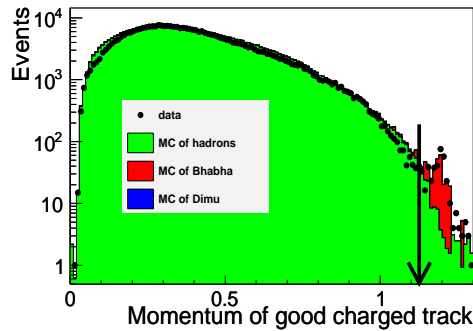


Figure 4: momentum distribution of tracks without maximum momentum requirement. The black dots are experimental data, green histogram is signal MC, red histogram is MC of Bhabha and blue histogram is MC of Dimu.

5 • Non-collision tracks (tracks other than electrons, muons, pions, kaons and protons) are removed  
 6 with

$$\chi = \frac{dE/dx_{measure} - dE/dx_{proton}}{\sigma_{proton}} > 10. \quad (2)$$

7 Figure 5 shows the scatter plot of  $dE/dx$  versus momentum for tracks (left) and distribution of  $\chi$   
 8 (right) at 2.4 GeV.

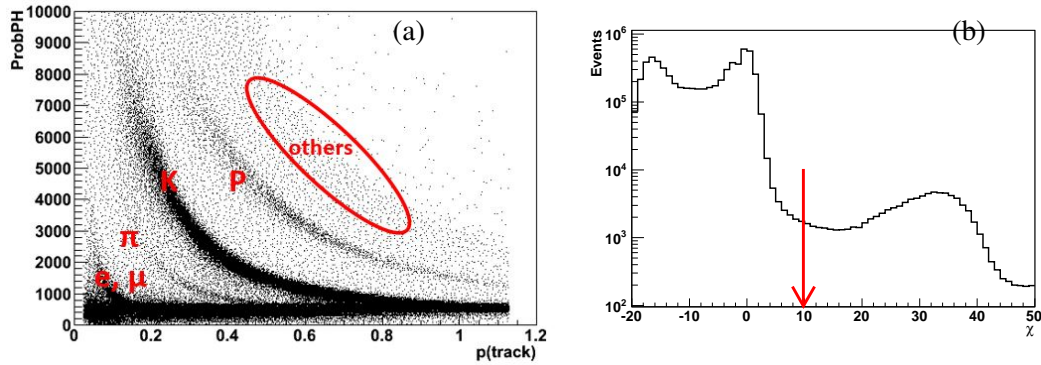


Figure 5: Scatter plot of  $dE/dx$  versus momentum (a) and distribution of  $\chi$  (b).

- 1 • Remove tracks with  $E/p > 0.8$  and  $p > 0.65 \times p_{beam}$ , where  $E$  is the energy deposition in EMC  
 2 and  $p$  represents the momentum measured by MDC. This requirement is applied to remove some  
 3 Bhabha events with a large energetic radiative photon.

4 Figure 6 shows the  $E/p$  distribution of tracks (left) and momentum distribution of tracks while  
 5 their  $E/p$  is larger than 0.8 (right) at 2.4 GeV.

6 Figure 7 shows the  $E/p$  distribution of tracks after applying this requirement. The peak around 1.0  
 7 is from radiative Bhabha, which can not be described well by MC.

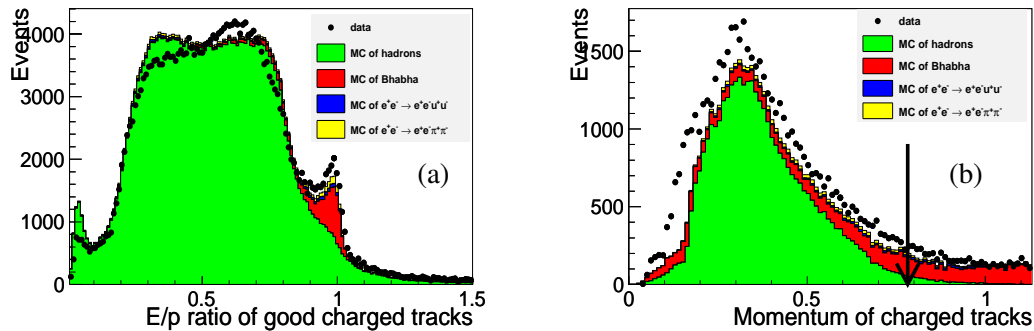


Figure 6:  $E/p$  ratio distributions of tracks (a) and momentum distribution (b). Where dots are data, and shade histograms are backgrounds from hadrons (green) and Bhabha (red) processes.

- 8 • Gamma-conversions ( $\gamma \rightarrow e^+e^-$ ) are removed if the invariant mass of an electron and positron pair  
 9 (tracks with  $E/p$  ratio larger than 0.8) is less than  $0.1 \text{ GeV}/c^2$  and their open angle is less than 15  
 10 degrees.

11 Figure 8 shows the scatter plot of  $M(e^+e^-)$  (invariant mass of electron and positron) versus  $Angle(e^+, e^-)$   
 12 (angle between electron and positron) at 2.4 GeV. Events in red box are regarded as gamma-  
 13 conversions.

- 14 • A neutral cluster is considered to be a good photon candidate if the following requirements are  
 15 satisfied: the deposited energy is larger than 25 MeV in the Barrel EMC ( $|\cos \theta| < 0.8$ ) or 50  
 16 MeV in the End-cap EMC ( $0.86 < |\cos \theta| < 0.92$ ); the angle between the cluster and the nearest

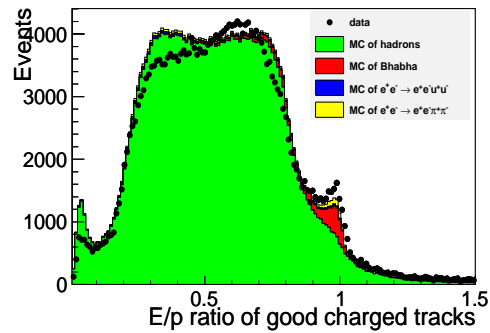


Figure 7:  $E/p$  ratio distributions of tracks after removing the large momentum electrons and positrons. Where dots are data, and shade histograms are backgrounds from hadrons (green) and Bhabha (red) processes.

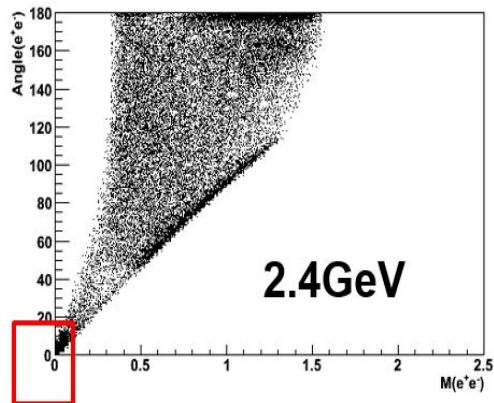


Figure 8: Scatter plot of  $M(e^+e^-)$  versus  $Angle(e^+e^-)$  at 2.4 GeV.

1 charged particle is larger than 20 degrees. In order to suppress electronic noise and energy deposits  
 2 unrelated with signal event, the time of EMC is required to be  $0 < t < 14$  [in unit of 50 ns].

### 3 4.3 Good Hadronic Event

4 After good charged tracks and good showers are selected, hadronic events are reconstructed with the  
 5 criteria as follows.

- 6 • The number of good hadronic track in an event is required to be larger than one. The total energy  
 7 deposition in EMC (sum of energy depositions for all good charged tracks and neutral ones) is  
 8 required to be larger than  $0.4 \times E_{beam}$  to remove non-collision background.

9 Figure 9 shows the distribution of total energy deposition in EMC at 2.4 GeV.

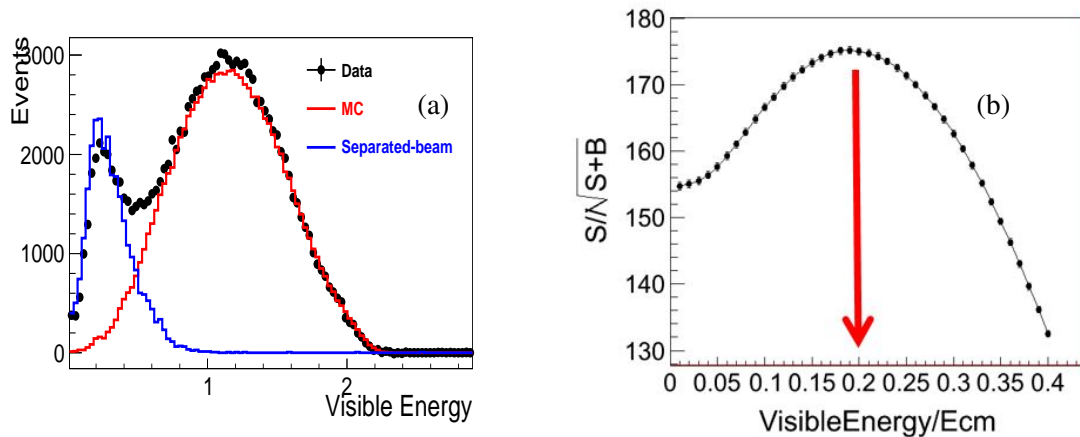


Figure 9: Distribution of total energy deposition in EMC (a) and the optimization distribution (b) at 2.4 GeV. Where black dots are experimental data, red histogram is MC of hadrons and blue histogram is separated beam data. Separated beam data is scaled to the same data taking time with collision data.

- 10 • If the number of good hadronic tracks in an event is two, the two tracks are required not to be  
 11 back-to-back within 10 degrees in  $\theta$  ( $|\Delta\theta| = |\theta_1 + \theta_2 - 180^\circ| < 10.0^\circ$ ) and 15 degrees in  $\phi$  ( $|\Delta\phi| =$   
 12  $||\phi_1 - \phi_2| - 180^\circ| < 15.0^\circ$ ). This requirement is applied to remove the Bhabha and Dimu events.  
 13 In addition, there must be at least two isolated photons. For each isolated photon, the energy is  
 14 required to be larger than 0.1 GeV and angle between the nearest good charged track is larger  
 15 than 20 degrees. In order to suppress electronic noise and energy depositions unrelated with signal  
 16 event, the time of EMC at  $0 < t < 14$  [in unit of 50 ns] is applied.

17 Figure 10 shows the  $|\Delta\theta|$  and  $|\Delta\phi|$  distributions (while the number of good hadronic track is two)  
 18 at 2.4 GeV.

19 Figure 11 shows the number of isolated photons distribution (while the number of good hadronic  
 20 track is two) at 2.4 GeV.

- 21 • If the number of good hadronic tracks in an event is three, the two largest energetic tracks must not  
 22 be back-to-back within 10 degrees in  $\theta$  ( $|\Delta\theta| = |\theta_1 + \theta_2 - 180^\circ| < 10.0^\circ$ ) and 15 degrees in  $\phi$  ( $|\Delta\phi| =$   
 23  $||\phi_1 - \phi_2| - 180^\circ| < 15.0^\circ$ ). Similarly, this requirement is applied to remove the Bhabha events.
- 24 • If the number of good hadronic tracks in an event is larger than three, no additional requirement is  
 25 applied.

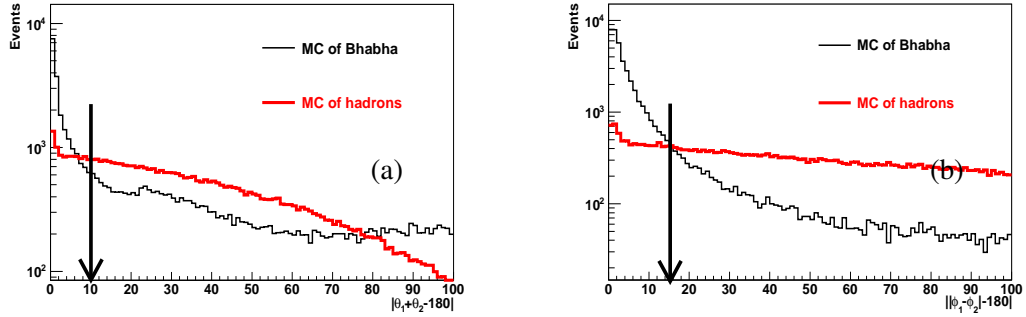


Figure 10:  $|\Delta\theta|$  (a) and  $|\Delta\phi|$  (b) distributions at 2.4 GeV. Black histograms are MC of hadrons and red ones are MC of Bhabha.

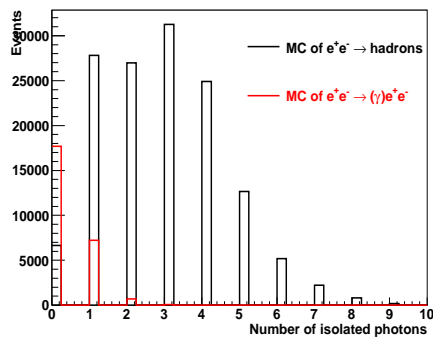


Figure 11: Number of isolated photons distribution for MC samples produced at 2.4 GeV. Black histogram is MC of  $e^+e^- \rightarrow$  hadrons and red one is MC of Bhabha.

## 5 Determination of number of hadronic events

After surviving all hadronic event selection criteria, the remaining backgrounds include two parts. One is the beam-associated backgrounds, such as beam-gas and beam-wall events. The other is QED backgrounds, such as Bhabha, Di-gamma,  $\mu^+\mu^-$ ,  $\tau^+\tau^-$  and  $e^+e^- + X$ .

### 5.1 Beam-associated Backgrounds

Beam-associated backgrounds, such as beam-gas and beam-wall events, are The main non-collisional backgrounds in hadronic events. The beam-gas events come from the reaction between the beam and the residual gas in the beam pipe. And the beam-wall events come from the reaction between the beam and the detector material. In order to simulate these events, the separated-beam data is taken.

The number of beam-associated background events is determined by fitting the distribution of event vertex in  $Z$  direction. For all events surviving the hadronic event selection criteria, the event vertex in  $Z$  direction ( $V_z$ ) is defined as

$$V_z = \frac{\sum_1^{N_{Good}} V_z(i)}{N_{Good}}, \quad (3)$$

where  $N_{Good}$  is the number of good hadronic tracks in one event. Here the absolute  $V_z$  is required to be less than 20 cm since almost all of the collisional events locate in this region.

For each energy point, the  $V_z$  distribution is fitted by using Monte Carlo shape convoluted with the Gaussian (signal) and 3rd order polynomial (beam-associated background) function. Figure 12 shows the fitting result at  $\sqrt{s} = 2.4$  GeV, and the fitting results at other energy points are listed in appendix ??.

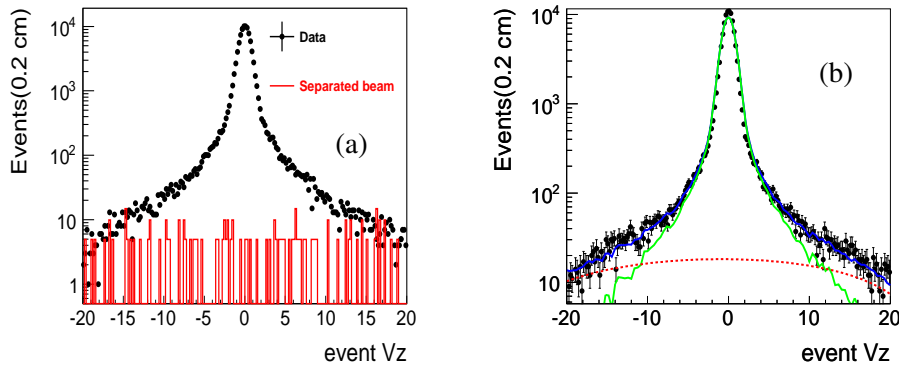


Figure 12: Event  $V_z$  distributions at 2.4 GeV (a). Black dots are collision data and red histograms are separated-beam data. The fitting results at 2.4 GeV (b). Blue lines represent signal and red lines are beam-associated background.

In order to validate the background shape can be described with a 3rd order polynomial function, the separated-beam data collected at 2.6444 GeV in 2015 is used. The comparison between data and separated-beam is shown in Figure 13, in which the separated-beam is scaled to the same data taking time as the collision data.

### 5.2 QED Backgrounds

In order to estimate the number from QED processes ( $(\gamma_{ISR})e^+e^-$ ,  $(\gamma_{ISR})\gamma\gamma$ ,  $(\gamma_{ISR})\mu^+\mu^-$ ,  $\tau^+\tau^-$  and  $e^+e^- + X$ ) that survive the hadronic event selection, MC samples of these processes are used. The same event selection is applied to these MC samples, and the number of survived events are scaled according to

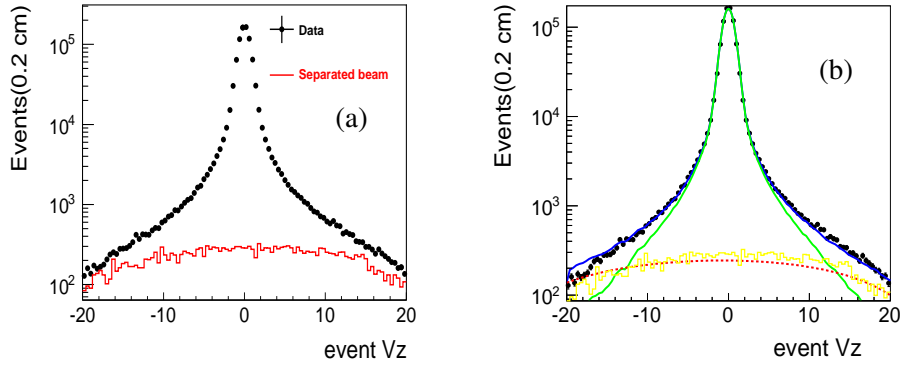


Figure 13: Event  $V_z$  distributions at 2.6444 GeV (a). Black dots are collision data and red histograms are separated-beam data. The fitting results at 2.6444 GeV (b) shows good agreement between the separated-beam (yellow histogram) and fitting background (red line).

- 1 the luminosity of experimental data. Table 3 shows the result of hadronic events and background events
- 2 estimation at all the energy points.
- 3 To cross check the estimation of QED background events, the MC samples of  $(\gamma_{ISR})e^+e^-$ ,  $(\gamma_{ISR})\gamma\gamma$
- 4 using generator BabayagaNLO and  $(\gamma_{ISR})\mu^+\mu^-$  using Phokhara9.1 have been used.

Table 3: Summary of hadronic events and background events estimation, here the numbers of background are normalized according to the data luminosity.

$\sqrt{s}(\text{GeV})$	Hadronic evnets from fitting	Bhabha	Di-gamma	$\mu^+\mu^-$	$e^+e^- + X$	$\tau^+\tau^-$	Final hadronic events
2.2324	90271±308	2222	123	108	24	–	87751±316
2.4000	104148±331	2472	120	107	11	–	101386±340
2.8000	89442±305	1917	90	94	17	–	87288±308
3.0500	299016±557	6386	302	335	256	–	291526±559
3.0600	298107±556	6373	270	333	280	–	290699±559
3.0800	583432±779	12988	603	710	552	–	568693±791
3.4000	33145±186	610	26	32	12	–	32449±193
3.5000	64771±259	1202	56	63	78	–	63347±264
3.5424	150110±394	2790	120	148	180	–	146801±398
3.5538	95893±316	1635	75	92	164	–	93710±317
3.5611	66419±263	1165	51	63	81	773	64249±273
3.6002	163944±413	2765	125	158	199	5525	155072±424
3.6500	80599±288	1413	58	79	41	4083	74904±292
3.6710	77001±282	1398	60	75	96	4221	71133±292

Table 4: Cross check of QED background estimation. The differences contributing to  $R$  are estimated.

$\sqrt{s}$ (GeV)	final hadronic events	Bhabha			Digamma			Dimu		
		3.5	NLO	Diff(%)	3.5	NLO	Diff(%)	3.5	Phokhara	Diff(%)
2.2324	87751	2222	1875	0.39	123	91	0.04	108	79	0.03
2.4000	101386	2472	1882	0.57	120	87	0.03	107	70	0.04
2.8000	87288	1917	1527	0.44	90	64	0.03	94	55	0.04
3.0500	291526	6386	4947	0.49	302	210	0.03	335	197	0.05
3.0600	290699	6373	4805	0.53	270	221	0.02	333	201	0.04
3.0800	568693	12988	10004	0.52	602	409	0.03	710	423	0.05
3.4000	32449	610	453	0.47	26	20	0.02	32	20	0.04
3.5000	63347	1202	877	0.51	56	38	0.03	63	37	0.04
3.5424	146801	2790	1932	0.58	120	83	0.02	148	86	0.05
3.5538	93710	1635	1263	0.39	75	52	0.02	92	55	0.04
3.5611	64249	1156	833	0.50	50	36	0.02	63	39	0.04
3.6002	155072	2765	2116	0.42	125	82	0.03	158	85	0.04
3.6500	74904	1413	1112	0.40	58	43	0.02	79	45	0.04
3.6710	71133	1398	953	0.62	59	42	0.02	75	45	0.04

### 5.3 Treatment of data samples at 3.65 GeV

During the data taking, the level of beam-associated background is related to the beam status. This kind of background dominates the uncertainty of the  $R$  value measurement. We found that the background level at different data taking time is significantly different at  $\sqrt{s} = 3.65$  GeV. As shown in Table 1, data samples at 3 energy points, 3.08, 3.5424 and 3.65 GeV, were taken in two run-intervals. But the beam-associated background level in 2009 is much different from that in 2013, so the two samples at  $\sqrt{s} = 3.65$  GeV have to be analysed separately. However, this phenomenon does not happen for data samples at  $\sqrt{s} = 3.08$  and 3.5424 GeV.

Figure 14 shows the distributions of total deposited energy at  $\sqrt{s} = 3.65$  GeV for data taken in 2009 and 2013, in which the lower peaks represent the distributions from beam-associated backgrounds and the higher ones are the signals. This distribution indicates the high level of beam associated backgrounds for the 2009 data. However, the distributions of total deposited energy at  $\sqrt{s} = 3.08$  and 3.5424 GeV are consistent, as shown in Figure 15.

In this analysis, the data sample at  $\sqrt{s} = 3.65$  GeV is decomposed into two sets, i.e., the 2013 data set with the luminosity of  $4.760 \text{ pb}^{-1}$ , and the 2009 data set with luminosity of  $43.625 \text{ pb}^{-1}$ . We apply the same selection criteria to the 2013 data sample at  $\sqrt{s} = 3.65$  GeV as those taken at other energy points. For 2009 data sample at  $\sqrt{s} = 3.65$  GeV, the hadronic event selection is almost the same as others but only without the total energy deposition requirement. The  $R$  value at  $\sqrt{s} = 3.65$  GeV is measured with 2013 data set, and the 2009 data set is used for cross check, as described in the appendix ??.

## 6 Comparisons Between Data and Monte Carlo

After the final event selection criteria are applied, the comparisons between data and MC (both for ConExc and LundArLw) at  $\sqrt{s}=2.4$  GeV are shown in Fig. 16 and Fig. 17. The comparison for other energy points are given in Appendix ??. The various comparison between data and MC include: (a) multiplicity of charged tracks, (b) multiplicity of neutral tracks, (c)  $\cos\theta$ , (d)  $\phi$ , (e) momentum of good

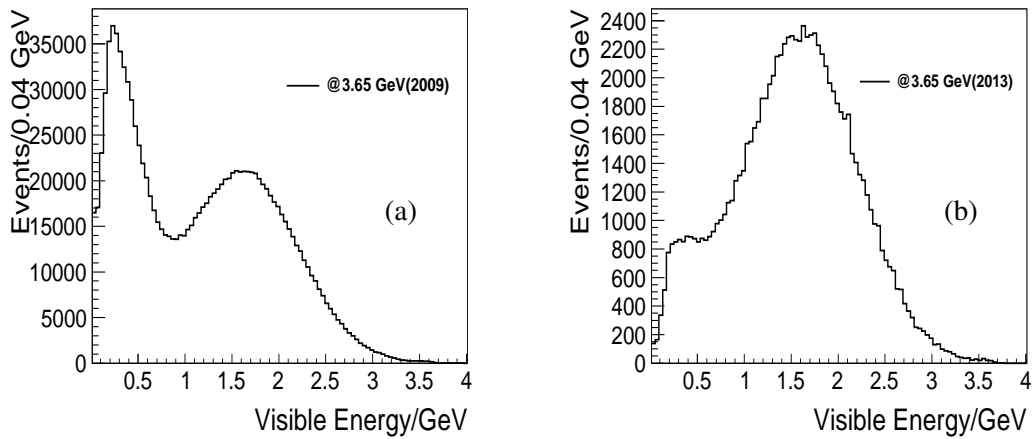


Figure 14: Distributions of total deposited energy at 3.65 GeV for data in 2009 (a) and 2013 (b).

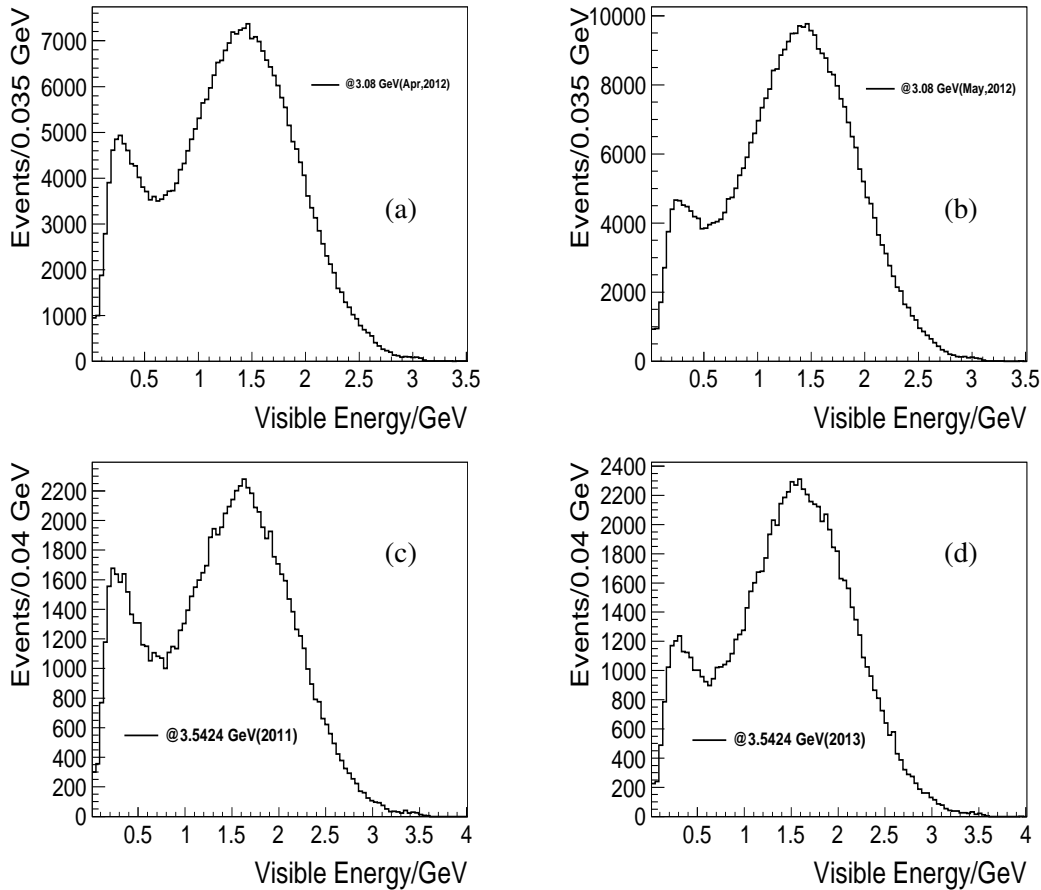


Figure 15: Distributions of total deposited energy at 3.08 GeV for data in April, 2012 (a), May, 2012 (b) and 3.5424 GeV for data in 2011 (c) and 2013 (d). They appear the similar distribution with a dip at around 0.5 GeV.

1 charged tracks, (f) energy deposition of good neutral tracks, (g) invariant mass of  $\pi^+\pi^-$  in the  $K_s^0$  mass  
 2 region, and (h) invariant mass of  $\gamma\gamma$  in the  $\pi^0$  mass region. The QED background has been subtracted  
 3 using MC samples after scaling to the same luminosity of experimental data.

## 4 7 Detection Efficiency

5 The detection efficiencies are determined with MC samples, in which the events are generated with the  
 6 generator model ConExc [17]. The ConExc model is constructed within the framework of BesEvtGen.  
 7 It provides momentum for each final state to do the detection simulation, and provide the initial state  
 8 radiation (ISR) factor and vacuum polarization factors for user to undress the observed cross section.  
 9 The basic idea of this generator is to decompose the total hadron cross section into the measured ones for  
 10 exclusive decays and the unknown part. The processes corresponding to the unknown part are generated  
 11 with the inclusive generator according to Lund area law (Lunda) model.

12 The ISR effects are included in the ConExc model, and the calculation of ISR factor is described  
 13 in the appendix. The input Born cross section below  $\sqrt{s} = 2.0$  GeV are quoted from PDG data, and  
 14 the Born cross section from  $\sqrt{s} = 2.0$  GeV to  $\psi(2S)$  peak are taken from this measurement. The ISR  
 15 factor is calculated based on the structure function method, and the radiator function is taken as the QED  
 16 calculation results up to the next-next-to-leading order. The ISR factor has been validated by comparing  
 17 those calculated by other generators, e.g., the KKMC and Phokhara (see Ref. [17]), and uncertainty  
 18 comparing to other calculation scheme are discussed in the appendix ??.

19 The vacuum polarization (VP) effects are also included in the ConExc model. Now there are many  
 20 groups to calculate the VP and available in literature. We use results provided by Fred Jegerlehner group  
 21 [22]. It provides leptonic and hadronic VP both in the space- and time-like region. For the leptonic  
 22 VP the complete one- and two-loop results and the known high-energy approximation for the three-loop  
 23 corrections are included. The hadronic contributions are given in tabulated form. The full set of routines  
 24 can be downloaded from Jegerlehners web page <http://www-com.physik.hu-berlin.de/~fjeger/>.

25 The cross sections exclusively measured for a few processes are taken from published literatures,  
 26 which includes seventy exclusive decays in total, with energy region covering a range from 0.3 GeV up  
 27 to  $\psi(2S)$  peak (see the summary in Ref [17]). The sum of these cross section are shown in Fig.18.

28 The angular distribution for ISR photons is implemented in the ConExc model, which is charac-  
 29 terized by the beam collinear distribution. Angular distributions for final hadron states, however, are  
 30 implemented only for two-body decays, namely,  $1 + \cos^2\theta$  for  $VP$  and  $B\bar{B}$  (where  $V$  denotes a vector  
 31 meson,  $P$  denotes a pseudoscalar meson,  $B$  denotes a baryon) modes, and  $1 - \cos^2\theta$  for  $PP$  modes.

32 The parameters for Lund area law model are optimized with the data taken at 3.6500 GeV, and  
 33 the values are given in the Tab.5. These parameters are validated at other energy points, and the MC  
 34 distributions are in good agreement with data distributions [23].

35 Table 6 and Figure 19 show the detection efficiencies determined from MC samples.

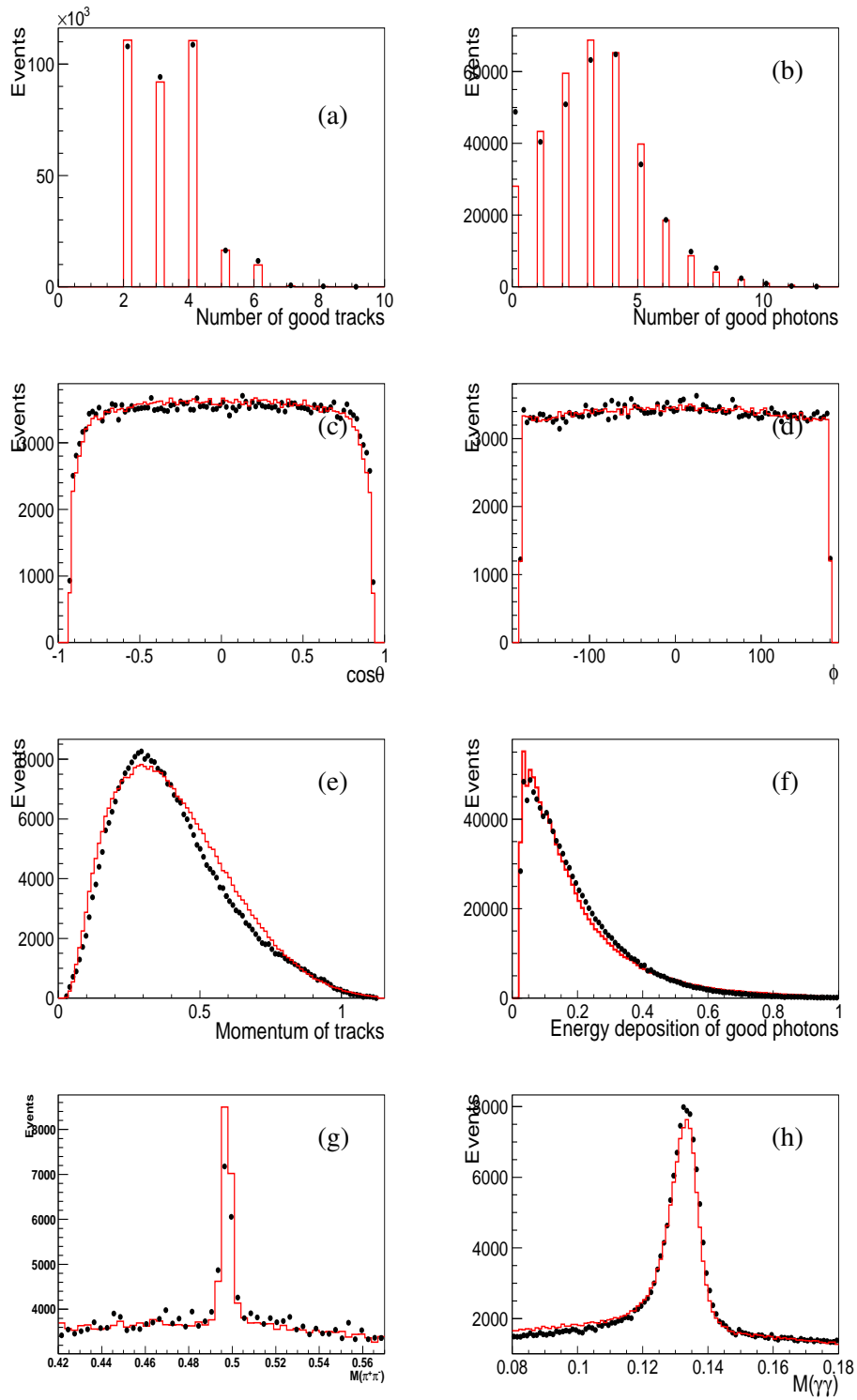


Figure 16: Comparisons between data and MC of ConExc at  $\sqrt{s} = 2.4$  GeV. In plots, the dots are data, and histogram is MC.

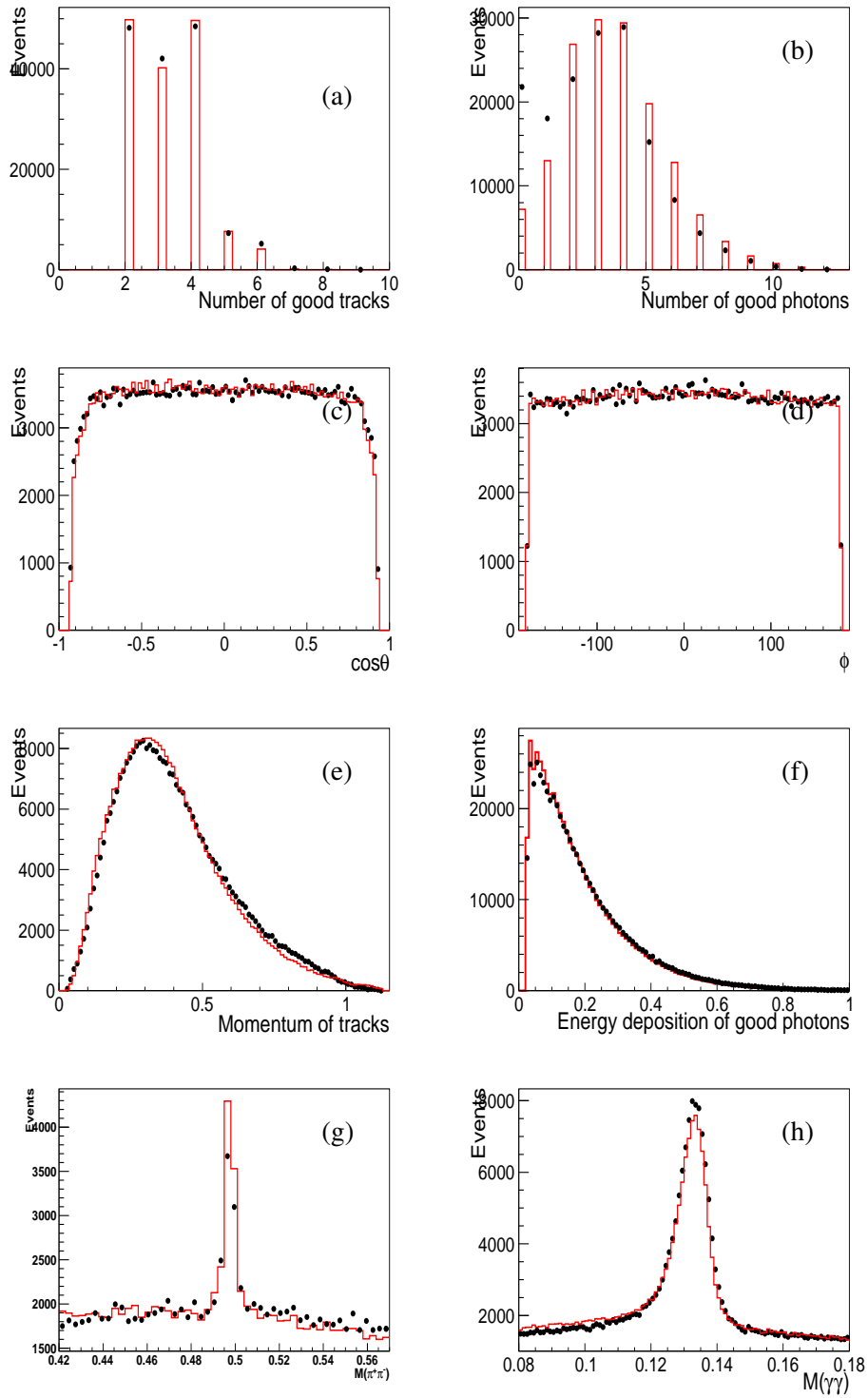


Figure 17: Comparisons between data and MC of LundArLw at  $\sqrt{s} = 2.4$  GeV. In plots, the dots are data, and histogram is MC.

Table 5: List of resulted parameters optimized with the data taken at  $\sqrt{s} = 3.6500$  GeV, the statistical errors are negligible.

Parameters	optimized	Description
PARJ(1)	0.065	P(qq)/P(q)
PARJ(2)	0.260	P(ss)/P(uu)
PARJ(11)	0.612	V/P ratio of u- and d-quarks
PARJ(12)	0.000	V/P ratio of s-quark
PARJ(14)	0.244	axial vector meson ratio
PARJ(15)	0.000	scalar meson ratio
PARJ(16)	0.437	another axial vector meson
PARJ(17)	0.531	tensor meson
PARJ(21)	0.066	$\sigma$ , width of Gaussian
RALPA(15)	0.577	LUNDA model parameter
RALPA(16)	0.365	LUNDA model parameter
RALPA(17)	0.000	LUNDA model parameter

Table 6: Summary of detection efficiency. The uncertainties are only statistical.

$E_{cm}$ (GeV)	Efficiency (%)
2.2324	71.00±0.50
2.4000	73.00±0.47
2.8000	76.86±0.50
3.0500	79.04±0.28
3.0600	79.15±0.28
3.0800	78.85±0.22
3.4000	79.66±0.78
3.5000	80.66±0.57
3.5424	80.47±0.40
3.5538	80.35±0.48
3.5611	80.41±0.57
3.6002	80.56±0.38
3.6500	81.78±0.53
3.6710	81.81±0.54

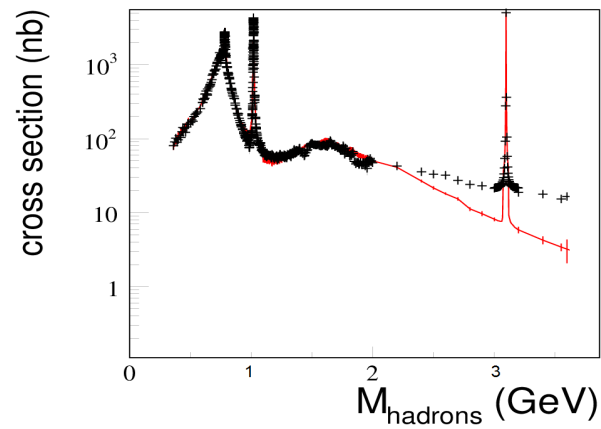


Figure 18: The Born cross section for light hadron production below  $\psi(2S)$  peak, where the black points with errors are the total hadron production [21], and the histogram with points (in red) is the sum of cross section for exclusive decays observed in experiments.

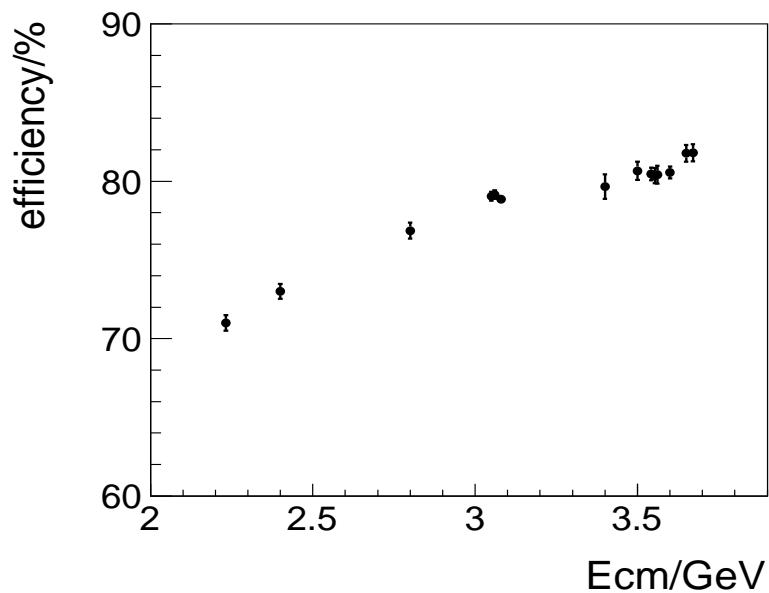


Figure 19: Detection efficiency of hadronic event selection. The uncertainties are only statistical.

## 8 The Initial State Radiation Correction

### 8.1 The ISR Correction

By definition,  $R$  value is the Born cross section  $\sigma_{had}^0$  in unit of the theoretic cross section  $\sigma_{\mu\mu}^0$  of  $e^+e^- \rightarrow \mu^+\mu^-$ , which corresponds to the tree level Feynman diagram of Fig.20(a). In experiment, the directly measured hadronic cross section is the total cross section  $\sigma_{had}^{tot}$ , which contains the total contributions of all Feynman diagrams shown in Fig.20(a-d). The ratio

$$\frac{\sigma_{had}^{tot}}{\sigma_{had}^0} \equiv (1 + \delta) \quad (4)$$

is called the ISR correction factor. With the help of the ISR theory, the factor  $(1 + \delta)$  can be calculated, and then  $R$  value can be obtained by the measured  $\sigma_{had}^{tot}$ :

$$R \equiv \frac{\sigma_{had}^0}{\sigma_{\mu\mu}^0} = \frac{\sigma_{had}^{tot}}{\sigma_{\mu\mu}^0(1 + \delta)}. \quad (5)$$

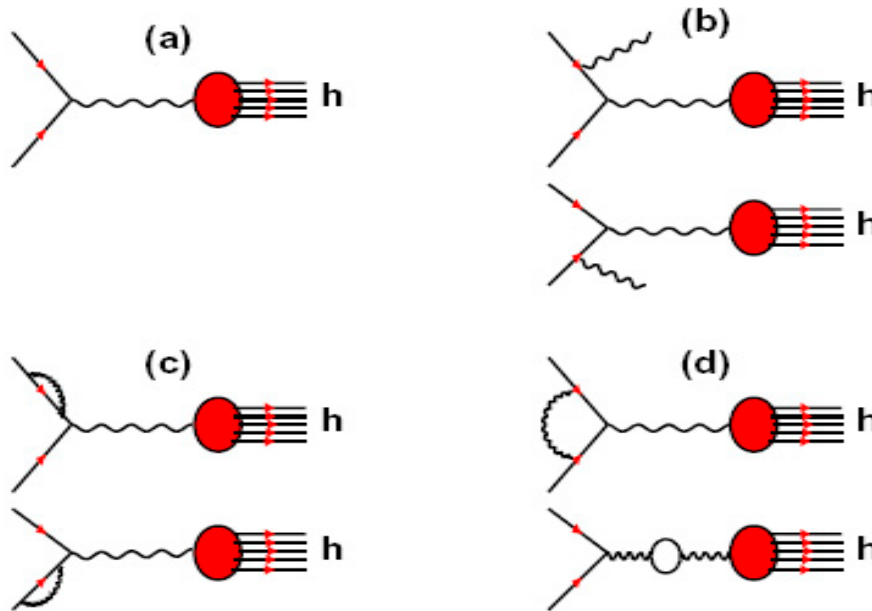


Figure 20: Feynman diagrams of ISR up to order  $O(\alpha^3)$ : (a) Born (tree level) diagram; (b) bremsstrahlung of real photon; (c) electron self-energy; (d) vertex correction and virtual photon vacuum polarization.

The calculation of ISR correction concerns the choice of theoretical schemes. In general, there are two classes of theoretic schemes for the calculations of the hadronic total cross section  $\sigma_{had}^{tot}$ , one is the calculations based on the Feynman diagram (FD) scheme[24, 25, 26, 27], another is the structure function (SF) scheme[28, 29] which is similar to that of the treatment of the Drell-Yan processes[32]. The precision of the FD scheme is determined by the the orders of the perturbative calculations. For example, the precision up to the one-loop calculations in Fig.20 is about  $O(\alpha) \sim 1\%$ , which fulfills the objective of this work. The issues of SF scheme applying to  $R$  value measurement are discussed in Appendix ???. After extensive studies and comparisons to these schemes, the values of  $(1 + \delta)$  calculated with the FD scheme are adopted in this work, and the calculation results of SF scheme are also given as a cross check.

1 The calculations of ISR factor  $(1 + \delta)$  used in the  $R$  value measurements with Crystalball (CB)  
 2 and BESII were described in references [26, 27] and [31]. It was assumed that all of the higher level  
 3 ISR correction terms corresponding to Fig.20(b,c,d) are smaller compared with the tree level term of  
 4 Fig.20(a), and then the VP factor  $1/|1 - \Pi(s)|^2$  was expressed as a Taylor series and taken the first  
 5 two terms only. Considering this assumption for VP factor around the narrow resonances like  $J/\psi$  and  
 6  $\psi(3686)$  be very rough, the VP factor should be recovered to its original form  $1/|1 - \Pi(s)|^2$ , see the  
 7 appendix. The more accurate formula for the total cross section can be written as

$$\sigma^{tot}(s) = (1 - x_m^\beta + \delta_{vert}) \frac{\sigma^0(s)}{|1 - \Pi(s)|^2} + \beta \int_0^{x_m} dx F_{FD}(x; s) \frac{\sigma^0(s')}{|1 - \Pi(s')|^2}, \quad (6)$$

8 where  $x$  is the energy fraction carried by the bremsstrahlung photon  $x = E_\gamma/E_{beam} = 2E_\gamma/\sqrt{s}$ , and the  
 9 upper limit of the integral  $x_m = 1 - 4m_\pi^2/s$  corresponds to the hadronic production threshold of the lightest  
 10 state  $e^+e^- \rightarrow \gamma\pi^+\pi^-$ , the function

$$F_{FD}(x; s) = \beta \frac{x^\beta}{x} \left(1 - x + \frac{x^2}{2}\right) \quad (7)$$

11 is called the radiator in FD scheme. In the calculations of Eq.(6), the Born sections  $\sigma^0(s)$  below 2 GeV  
 12 uses the PDG values which contain the contributions from both continuous and resonant states, and the  
 13 integrand above 2 GeV uses following expression

$$\frac{\sigma^0(s)}{|1 - \Pi(s)|^2} = \sigma_{\mu\mu}^0(s) \frac{R_{datfit}(s)}{|1 - \Pi(s)|^2} + \frac{12\pi}{|1 - \Pi_0(s)|^2} \sum_{i=J/\psi, \psi'} \frac{\Gamma_{ei}^0 \Gamma_i}{(s - M_i^2)^2 + M_i^2 \Gamma_i^2}. \quad (8)$$

14 The values of  $R_{datfit}(s)$  are obtained by iteratively fitting the  $R$  values between 2.2324-3.671 GeV mea-  
 15 sured in this work. The calculations of VP factors  $\Pi(s)$  and  $\Pi_0(s)$  can bound in Appendix ???. The  
 16 numerical results calculated with Eq.(6) are marked as CB, which means it was ever used by Crystalball  
 17 Group.

## 18 8.2 The Numerical Results

19 The energy dependence of inclusive hadronic cross section  $\sigma^0(s)$ ,  $\sigma^{tot}(s)$  and ISR factor  $(1 + \delta)$  are  
 20 calculated using the FD (CB) and SF (marked as WU and KF) schemes respectively, the numerical  
 21 results of CB, WU and KF are shown in Fig.21 for comparisons. The more detail descriptions can be  
 22 found in the appendix.

23 The calculation error of the ISR factor  $\Delta_{FD}$  can be estimated from three sides: (1) the uncertainty  
 24 of the one-loop perturbative calculations  $\Delta_{order}$  ( $\sim \mathcal{O}(\alpha) \sim 1\%$ ); (2) the errors induced by the input  
 25 Born cross sections  $\Delta_{\sigma^0}$  ( $\sim 0.1 - 0.8\%$ ), see Table ???; (3) the errors induced by VP factor uncertainty  
 26  $\Delta_{VP}$  ( $\sim 0.2 - 0.6\%$ ), see Table ???. For the FD scheme, the systematic error is estimated by

$$\Delta_{FD}^2 = \Delta_{order}^2 + \Delta_{\sigma^0}^2 + \Delta_{VP}^2. \quad (9)$$

27 The values and errors of  $(1 + \delta)$  at the energy points in this work are shown in Table 7.

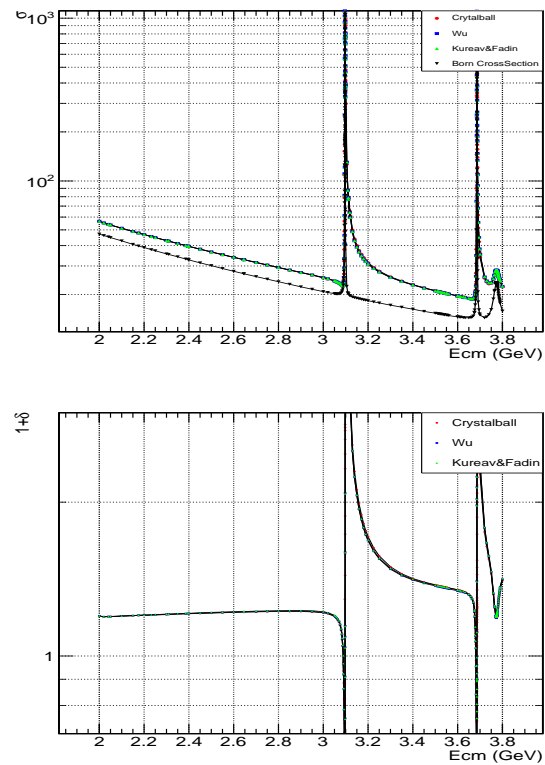


Figure 21: Left: The Born cross section (black triangle) and total cross section calculated by CrystalBall scheme (red circle), WU's scheme (blue square), Kureav and Fadin's scheme (green triangle); Right: The ISR factors calculated by the Crystalball scheme (red circle), WU's scheme (blue square), Kureav and Fadin scheme (green triangle).

Table 7: The ISR factor ( $1 + \delta$ ) calculated by Eq.(6), and the composed errors estimated by Eq.(9). The values in the blanket are the relative errors.

$\sqrt{s}(\text{GeV})$	CB
2.2324	1.190±0.015 (1.25%)
2.4000	1.195±0.015 (1.22%)
2.8000	1.224±0.014 (1.17%)
3.0500	1.195±0.013 (1.12%)
3.0600	1.183±0.013 (1.12%)
3.0800	1.124±0.013 (1.16%)
3.4000	1.403±0.015 (1.07%)
3.5000	1.366±0.018 (1.29%)
3.5424	1.354±0.017 (1.25%)
3.5538	1.351±0.017 (1.22%)
3.5611	1.349±0.017 (1.22%)
3.6002	1.348±0.016 (1.20%)
3.6500	1.339±0.016 (1.23%)
3.6710	1.285±0.015 (1.15%)

Table 8: Summary of systematic uncertainty from event selection. For alternative cuts, the uncertainties at the both end are checked, and the larger one is taken as the systematic uncertainty.

Source	Cut	Default	Alternative	Uncertainty (%)
veto Bhabha and $\gamma\gamma$	$E_{ratio}$	$0.65 \cdot E_{beam}$	$0.6 \sim 0.7 \cdot E_{beam}$	0.09
	$\Delta\theta$	$10^\circ$	$5^\circ \sim 15^\circ$	0.04
good hadronic tracks determination	$Vr$	1.0 cm	0.5 cm	0.36
	$p(track)$	$0.94 \cdot p_{beam}$	$0.92 \sim 0.96 \cdot p_{beam}$	0.01
	$dE/dx$ cut	10	15	0.02
	$E/p$ ratio	0.8	$0.75 \sim 0.85$	0.39
	Bhabha momentum limit	$0.65 \cdot p_{beam}$	$0.6 \sim 0.7 \cdot p_{beam}$	0.79
	isolated photon angle	$20^\circ$	$15^\circ \sim 25^\circ$	0.11
	isolated photon energy	100 MeV	$75 \sim 125$ MeV	0.77
	gamma conversion angle	$15^\circ$	$10^\circ \sim 20^\circ$	0.10
gamma conversion mass	100 MeV	$80 \sim 120$ MeV	0.10	
visible energy	total energy deposition	$0.4 \cdot E_{beam}$	$0.35 \sim 0.45 \cdot E_{beam}$	0.12
2 prong events	$\Delta\theta$	$15^\circ$	$10^\circ \sim 20^\circ$	0.04
	$\Delta\phi$	$10^\circ$	$5^\circ \sim 15^\circ$	0.15
>2 prong events	$\Delta\theta$	$15^\circ$	$10^\circ \sim 20^\circ$	0.07
	$\Delta\phi$	$10^\circ$	$5^\circ \sim 15^\circ$	0.07
others	weighting method(Appendix ??)	2 dimension	1 dimension	0.50
	QED background			0.01
total				1.36

## 9 Systematic Uncertainty

We consider the systematic uncertainties associated with the event selection, luminosity, detection efficiency, radiative correction factor and trigger efficiency, respectively.

According to definition of  $R$  value in Eq. (1), its systematic uncertainty is calculated by

$$\left(\frac{\Delta R}{R}\right)_{sys.} = \left\{ \left(\frac{\Delta \tilde{N}}{\tilde{N}}\right)_{had}^2 + \left(\frac{\Delta \mathcal{L}}{\mathcal{L}}\right)_{sys.}^2 + \left(\frac{\Delta \varepsilon_{had}}{\varepsilon_{had}}\right)^2 + \left[\frac{\Delta(1+\delta)}{(1+\delta)}\right]^2 + \left(\frac{\Delta \varepsilon_{trig}}{\varepsilon_{trig}}\right)^2 \right\}^{1/2}, \quad (10)$$

the terms in the right side of above equation represent the contributions from hadronic event selection, integrated luminosity, efficiency from different generator models, initial state radiation correction and trigger efficiency, respectively.

### 9.1 Event Selection

The uncertainties associated with the hadronic event selection criteria are estimated with alternative ones, as listed in Table 8. We re-estimate the number of hadronic events and detection efficiency by replacing a given cut with the alternative one, and  $R$  value is obtained. The difference of  $R$  value between that obtained with the default and alternative cuts is taken as the systematic uncertainty. The uncertainty associated with each cut is estimated one by one. Table 8 gives the alternative cuts and the corresponding systematic uncertainties at 2.2324 GeV.

## 1 9.2 Luminosity

2 The uncertainty from integrated luminosity measurement using  $e^+e^- \rightarrow (\gamma_{ISR})e^+e^-$  events is estimat-  
3 ed to be 1.0% [15].

## 4 9.3 Generator Model

5 The detection efficiencies are determined with the MC samples generated with the ConExc model.  
6 The uncertainties associated with the generator model are estimated with those MC samples generated  
7 with the Lund Area Law model (LUARLW). The differences between them are taken as the systematic  
8 uncertainties from the generator model.

9 Table 9 lists detection efficiencies determined from two MC samples with two groups of parameters.

Table 9: Summary of systematic uncertainty from generator model.

$E_{cm}(\text{GeV})$	Efficiency (ConExc)	Efficiency (LUARLW)	Uncertainty (%)
2.2324	71.00	72.35	1.93
2.4000	73.00	75.09	2.84
2.8000	76.86	78.66	2.22
3.0500	79.04	79.98	1.12
3.0600	79.15	79.75	0.67
3.0800	78.85	79.64	0.87
3.4000	79.66	80.07	0.32
3.5000	80.66	80.01	0.87
3.5424	80.47	79.94	0.83
3.5538	80.35	79.66	1.04
3.5611	80.41	79.86	0.74
3.6002	80.56	79.69	1.26
3.6500	81.78	80.47	1.60
3.6710	81.81	80.50	1.66

10

## 11 9.4 Radiation Correction

12 The radiation correction factor we used is calculated via the Feynman diagram scheme (see appendix  
13 ??). As a cross check, the structure function scheme is also applied (see appendix ??). The results are  
14 listed in Table 10. The differences between these two methods are also listed in this table for a cross  
15 check, and the details are given in appendix ??.

## 16 9.5 Trigger Efficiency

17 The trigger efficiency for barrel  $e^+e^- \rightarrow$  hadrons events approaches 100% with an uncertainty less  
18 than 0.1% [14].

## 19 9.6 Total Systematic Uncertainty

20 Table 11 summarizes all systematic uncertainties under consideration.

Table 10: Systematic uncertainty from radiation correction factor.

$\sqrt{s}$ (GeV)	ISR (Feynman diagram)	ISR (structure function)	Difference (%)
2.2324	1.190±0.015 (1.25%)	1.197	0.59
2.4000	1.195±0.015 (1.22%)	1.204	0.75
2.8000	1.224±0.014 (1.17%)	1.235	0.90
3.0500	1.195±0.013 (1.12%)	1.208	1.09
3.0600	1.183±0.013 (1.12%)	1.197	1.35
3.0800	1.124±0.013 (1.16%)	1.146	1.92
3.4000	1.403±0.015 (1.07%)	1.409	0.42
3.5000	1.366±0.018 (1.29%)	1.388	1.58
3.5424	1.354±0.017 (1.25%)	1.370	1.90
3.5538	1.351±0.017 (1.22%)	1.371	1.46
3.5611	1.349±0.017 (1.22%)	1.365	1.90
3.6002	1.348±0.016 (1.20%)	1.354	0.44
3.6500	1.339±0.016 (1.23%)	1.340	0.07
3.6710	1.285±0.015 (1.15%)	1.313	2.13

Table 11: Summary of systematic uncertainties. All the results are in percentage.

$\sqrt{s}$ (GeV)	event selection	luminosity	generator model	ISR correction factor	trigger efficiency	total
2.2324	1.36	1.00	1.93	1.25	0.10	2.85
2.4000	1.44	1.00	2.84	1.22	0.10	3.55
2.8000	1.40	1.00	2.22	1.17	0.10	3.04
3.0500	1.37	1.00	1.12	1.12	0.10	2.32
3.0600	1.40	1.00	0.67	1.12	0.10	2.16
3.0800	1.44	1.00	0.87	1.16	0.10	2.27
3.4000	1.29	1.00	0.32	1.07	0.10	1.98
3.5000	1.22	1.00	0.87	1.29	0.10	2.22
3.5424	1.24	1.00	0.83	1.25	0.10	2.19
3.5538	1.30	1.00	1.04	1.22	0.10	2.29
3.5611	1.24	1.00	0.74	1.22	0.10	2.14
3.6002	1.39	1.00	1.26	1.20	0.10	2.45
3.6500	1.40	1.00	1.60	1.23	0.10	2.65
3.6710	1.31	1.00	1.66	1.15	0.10	2.61

## 10 Results

The measured  $R$  values for the 14 energy points are shown in Fig. 22. The total uncertainties are the combination of statistical and systematic uncertainties in quadrature. Numerical results of measured  $R$  values are summarized in Table 12, where  $N_{had}^{obs}$  is the number of selected hadronic events, and  $N_{bkg}$  is the number of beam-associated background events obtained from fitting to the distribution of event  $V_z$ . The number of residual QED background events,  $N_{QED}$ , are subtracted using MC samples. They are mainly from the  $(\gamma_{ISR})e^+e^-$  and  $\tau^+\tau^-$  events, and a few from  $(\gamma_{ISR})\gamma\gamma$ ,  $\mu^+\mu^-$  and  $e^+e^- + X$  events. The luminosity ( $\mathcal{L}$ ), detection efficiency ( $\epsilon_{had}$ ) and ISR factor ( $1 + \delta$ ).

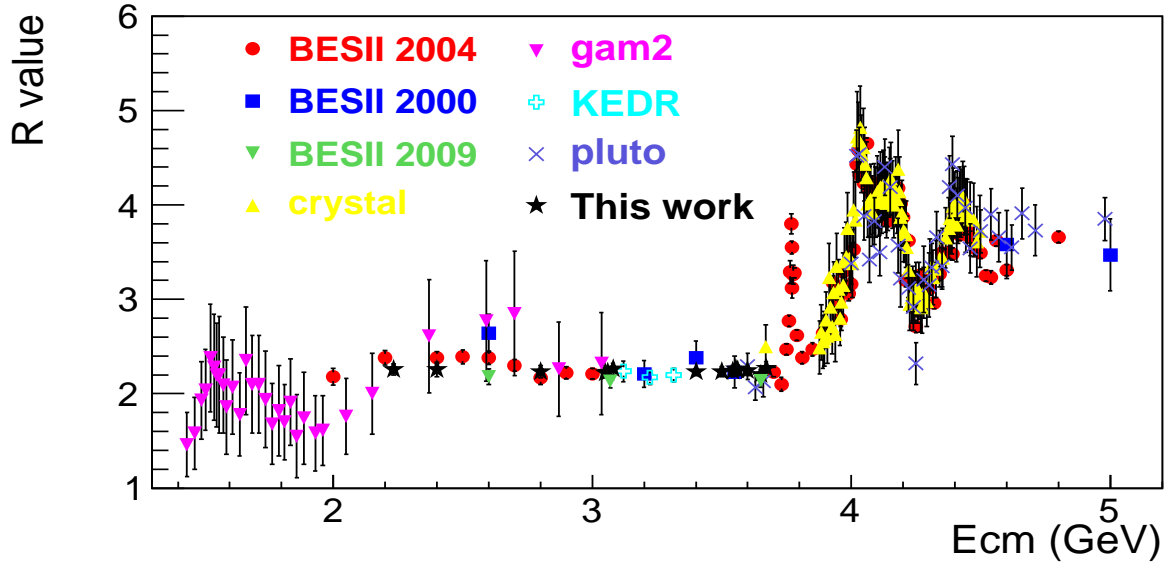


Figure 22: A compilation of measurement of  $R$  values in the center-of-mass energy range from 1.4 to 5 GeV. The dots with error bars marked as pentastar is the results in this analysis. The average uncertainty is about 3%.

Table 12: Summary of  $R$  value measurement.

$\sqrt{s}$ (GeV)	#events	$\epsilon_{had}$ (%)	$\mathcal{L}$ ( $\text{pb}^{-1}$ )	$1 + \delta$	$R$ value	Statistic uncertainty	Systematic uncertainty
2.2324	87751±316	71.00	2.645	1.190	2.254	0.009(0.40%)	0.064(2.85%)
2.4000	101386±340	73.00	3.415	1.195	2.258	0.008(0.38%)	0.080(3.55%)
2.8000	87288±308	76.86	3.753	1.224	2.233	0.009(0.39%)	0.068(3.04%)
3.0500	291526±559	79.04	14.893	1.195	2.221	0.005(0.22%)	0.052(2.32%)
3.0600	290699±559	79.15	15.040	1.183	2.227	0.005(0.22%)	0.048(2.16%)
3.0800	568693±791	78.85	31.019	1.124	2.261	0.004(0.16%)	0.051(2.27%)
3.4000	32449±193	79.66	1.733	1.403	2.231	0.014(0.62%)	0.044(1.98%)
3.5000	63347±264	80.66	3.633	1.366	2.232	0.010(0.44%)	0.050(2.22%)
3.5424	146801±398	80.47	8.693	1.354	2.240	0.007(0.31%)	0.049(2.19%)
3.5538	93710±317	80.35	5.562	1.351	2.262	0.008(0.37%)	0.052(2.29%)
3.5611	64249±273	80.41	3.847	1.349	2.248	0.010(0.45%)	0.048(2.14%)
3.6002	155072±424	80.56	9.502	1.348	2.243	0.007(0.31%)	0.055(2.45%)

Table 12: (continued) Summary of  $R$  value measurement.

$\sqrt{s}$ (GeV)	#events	$\epsilon_{had}$ (%)	$\mathcal{L}$ ( $\text{pb}^{-1}$ )	$1 + \delta$	$R$ value	Statistic uncertainty	Systematic uncertainty
3.6500	74904 $\pm$ 288	81.78	4.760	1.339	2.204	0.009(0.41%)	0.059(2.65%)
3.6710	71133 $\pm$ 292	81.81	4.628	1.285	2.270	0.010(0.44%)	0.059(2.61%)

## 11 Summary

The  $R$  values at 14 energy points between  $\sqrt{s} = 2.2324$  to 3.671 GeV are measured. The achieved precision for most measurements are better than 3%, and the uncertainties are dominated by the systematic errors. Compared to the BESII results [7], they are consistent within one standard deviation. Our measurements provide more  $R$  values in this energy region.

## References

- [1] P. A. Rapidis et al., Phys. Rev. Lett. **39**, 526 (1977)
- [2] J. Burmester et al., Phys. Lett. B **66**, 395 (1977)
- [3] R. H. Schindler et al., Phys. Rev. D **21**, 2716 (1980)
- [4] J. L. Siegrist et al., Phys. Lett. B **26**, 969 (1982)
- [5] J. Z. Bai et al.(BES Collaboration), Phys. Rev. Lett. **84**, 594 (2000)
- [6] J. Z. Bai et al.(BES Collaboration), Phys. Rev. Lett. **88**, 101802 (2002)
- [7] M. Ablikim et al.(BES Collaboration), Phys Lett. B. **677**(2009)239-245.
- [8] arXiv:1510.02667[hep-ex]
- [9] M. Ablikim *et al.* (BESIII Collaboration), Nucl. Instrum. Meth. A **614**, 345 (2010).
- [10] M. Ablikim *et al.* (BESIII Collaboration), Chin. Phys. C **37**, 032007 (2013).
- [11] G. Balossini, C. M. C. Calame, G. Montagna, O. N. F. Piccinini, Nucl. Phys. B **758**, 227 (2006).
- [12] S. Jadach, B. F. L. Ward and Z. Was, Comp. Phys. Commu. 130, 260 (2000); Phys. Rev. D. **63**, 113009 (2001).
- [13] DELPHI collaboration, DELPHI 90-35 PROG 152 (1990).
- [14] N. Berger, Zhu Kai et al. Chin. Phys. C **34**, 1779 (2010).
- [15] Zhen Gao, et. al., BAM-00157, Measurement of luminosity for R scan.
- [16] Li W D, Liu H M et al. The Offline Software for the BES-III (2006) Experiment, Proceeding of CHEP06 (Mumbai, India, 13-17 February 2006).
- [17] R. G. Ping et al. An exclusive event generator for  $e^+e^-$  scan experiment, Chin. Phys. C **38**, 083001 (2014).
- [18] B. Andersson, The Lund Model, Cambridge University Press, 1998.
- [19] B. Andersson, H. Hu, hep-ph/9810285.
- [20] B. Andersson, H. Hu, "Few-body States in Lund String Fragmentation Model", hep-ph/9910285.
- [21] K. A. Olive, et. al., (Particle data group) Chin. Phys. C **38**, 090001 (2014).

- 1 [22] S. Eidelman, F. Jegerlehner, Z. Phys. C 67, 585 (1995). hep-ph/ 9502298;  
2 F. Jegerlehner, Nucl. Phys. Proc. Suppl. 162, 22 (2006). hep-ph/ 0608329;  
3 F. Jegerlehner, Nucl. Phys. Proc. Suppl. 181C182, 135 (2008). 0807.4206;  
4 F. Jegerlehner, Nucl. Phys. Proc. Suppl. 126, 325 (2004). hep-ph/ 0310234;  
5 F. Jegerlehner, hep-ph/0308117 (2003).
- 6 [23] see talk by Ping Ronggang at BESIII workshop 2015, IHEP.  
7 <http://indico.ihep.ac.cn/event/5099/session/12/contribution/40/material/slides/0.pdf>
- 8 [24] G. Bonneau, F.Martin, Nucl. Phys. B27, 381(1971)
- 9 [25] F.A. Berends and Kleiss, Nucl. Phys. B187, 141(1981)
- 10 [26] A.Osterheld, et al. SLAC-PUB-4160(1986)(T/E)
- 11 [27] C.Edward,et al. SLAC-PUB-5160(1990)(T/E)
- 12 [28] E.A.Kureav and V.S.Fadin, Sov. J. Nucl. Phys. 41, 466(1985)
- 13 [29] J. Wu, Chinese Physics C (HEP NP)14, 585(1990) (in Chinese)
- 14 [30] S. Eidelman, F. Jegerlehner, Z. Phys. C 67, 585 (1995). hep-ph/ 9502298;  
15 F. Jegerlehner, Nucl. Phys. Proc. Suppl. 162, 22 (2006). hep-ph/ 0608329;  
16 F. Jegerlehner, Nucl. Phys. Proc. Suppl. 181C182, 135 (2008). 0807.4206;  
17 F. Jegerlehner, Nucl. Phys. Proc. Suppl. 126, 325 (2004). hep-ph/ 0310234;  
18 F. Jegerlehner, hep-ph/0308117 (2003).
- 19 [31] H. Hu et al. Chinese Physics C (HEP NP)25, 701(2001) (in Chinese)
- 20 [32] S.D.Drell and T.M.Yan, Ann. Phys. (N.Y) 66, 578(1971)
- 21 [33] O.Ncronisi and L.Trentadue, Nucl. Phys. B318, 1(1989)
- 22 [34] O.Ncronisi and L.Trentadue, Phys. Lett. B196, 551(1987)
- 23 [35] Particle Data Group, Chinese Physics C38, (1014)
- 24 [36] A.G.Shamov (KEDR Collaboration), CPC(HEP NP)34, 836(2009)
- 25 [37] S.G.Gorishnii et al. Phys. Lett. B259, 144(1991)
- 26 [38] Particle Data Group, Chinese Physics C38, (1014)
- 27 [39] M.E. Peskin and Daniel V. Schroeder, An Introduction to Quantum Field Theory, page175
- 28 [40] Y.S.Tsai, SLAC-PUB-3129, (1983)(T/E)
- 29 [41] A.G.Shamov, (KEDR Collaboration), CPC( HEP& NP) B34, 836(200)
- 30 [42] W.Greiner, J.Reinhardt, Quantum Electrodynamics. Springer, Berlin, 2002, 292
- 31 [43] G.Altarelli et al. Z Physics at LEP1, Volume 3: Event Generator and Software
- 32 [44] A.G.Shamov (KEDR Collaboration), CPC(HEPNP) 34, 836(2009)
- 33 [45] G.Bonvicini, Nucl. Phys. B323, 253(1989)
- 34 [46] M.Ablikim et al. (BES Collaboration), Phys. Lett. B660, 315(2008)